

Sensing with near-infrared laser trapped fluorescent nanodiamonds

Arthur Dervillez^{1,*}, Fatemeh Kalantarifard^{1,3}, Luca Troise¹, Alexander Huck², and Kirstine Berg-Sørensen^{1†}

¹ *Health Technology, DTU, Bygning, Ørstedes Pl. 345C, 2800 Kongens Lyngby, Denmark*

² *Departement of Physics, DTU, Fysikvej, building 311, 2800 Kongens Lyngby, Denmark and*

³ *Current affiliation: Department of Natural and Mathematical Sciences, Ozyegin University, 34794 Istanbul, Turkey*

(Dated: January 14, 2025)

Biosensing based on optically trapped fluorescent nanodiamonds is an intriguing research direction potentially allowing to resolve biochemical processes inside living cells. Towards this goal, we investigate infrared near (NIR) laser irradiation at 1064 nm on fluorescent nanodiamonds (FNDs) containing nitrogen-vacancy (NV) centers. By conducting comprehensive experiments, we aim to understand how NIR exposure influences the fluorescence and sensing properties of FNDs and to determine the potential implications for the use of FNDs in various sensing applications. The experimental setup involved exposing FNDs to varying intensities of NIR laser light and analyzing the resultant changes in their optical and physical properties. Key measurements included T_1 relaxation times, optical spectroscopy, and optically detected magnetic resonance (ODMR) spectra. The findings reveal how increased NIR laser power correlates with alterations in ODMR central frequency but also that charge state dynamics under NIR irradiation of NV centers plays a role. We suggest protocols with NIR and green light that mitigate the effect of NIR, and demonstrate that FND biosensing works well with such a protocol.

Keywords: Nanodiamond, Optical trapping, Temperature sensing, NV-centers

I. INTRODUCTION

Fluorescent nanodiamonds (FNDs) containing Nitrogen-Vacancy (NV) centers have attracted significant interest due to their combined optical and magnetic properties, which render them highly versatile for applications in particular in biomedical sensing and imaging [1, 2]. The capacity of NV centers for optical polarization and readout of spin states earmarks them as formidable tools for advanced sensing applications [3]. Yet, the utility of these sensors is heavily influenced by the photodynamics of the NV centers' spin- and charge-states, which in turn governs their sensitivity and accuracy [4].

NV centers possess an electronic spin $S=1$ system, characterized by spin sublevels $m_s = 0$ and $m_s = \pm 1$, which are separated by a zero-field splitting due to spin-spin interaction. This zero-field splitting is sensitive to external parameters such as temperature, strain, and electric fields, while the energies of the spin sublevels can be further shifted by magnetic fields through the Zeeman effect [5, 6]. Additionally, the optical spectrum of NV centers, including their fluorescence intensity and wavelength, is determined by the charge state distribution and depends on the local electrochemical potential and intrinsic charge state dynamics. These dependencies allow NV centers to act as versatile nanoscale sensors, providing insights into local magnetic fields across various frequency ranges, temperature fluctuations, and surface electrochemical conditions. Therefore, to accurately measure external parameters like magnetic fields

or temperature with high sensitivity in biological environments, it is essential to understand how external control—such as a near infrared trapping laser—affect the intrinsic properties of NV centers [7, 8].

Trapping of FNDs with optical tweezers is an attractive approach as it potentially allows for spatially resolved sensing in challenging environments, with a resolution determined by the size of the FND and of the trapping potential [9]. To achieve this in biological samples and minimize cell and tissue damage, the wavelength of the intense trapping laser must be in the biological transparency window, such as 1064 nm, where residual absorption of tissue components is minimal [10].

In this work, we employed three principal methods to investigate the properties of NV centers in FNDs under NIR light exposure: spin polarization relaxometry (T_1 -relaxometry) [11, 12], optically detected magnetic resonance (ODMR) spectroscopy [13, 14], and photoluminescence (PL) spectrum analysis [15]. PL spectroscopy involves measuring the emitted light from the NV centers when excited by a laser, providing information on the optical properties and charge states of the NV centers [16]. ODMR combines optical and microwave techniques to detect changes in the NV centers' fluorescence in response to varying magnetic fields and relative temperature changes, allowing for precise measurement of the NV centers' electron spin states and local magnetic environment [17]. T_1 -relaxometry, on the other hand, measures the longitudinal relaxation time (T_1), which is the time it takes for the NV centers' spin states to return to thermal equilibrium after being polarized [18]. This method is valuable for sensing processes and can detect various types of magnetic noise at the spin-transition frequency, such as free radicals [12]. Combined, these techniques provide a comprehensive analysis of the NV centers' optical, magnetic, and spin properties under vary-

* artde@dtu.dk

† kibs@dtu.dk

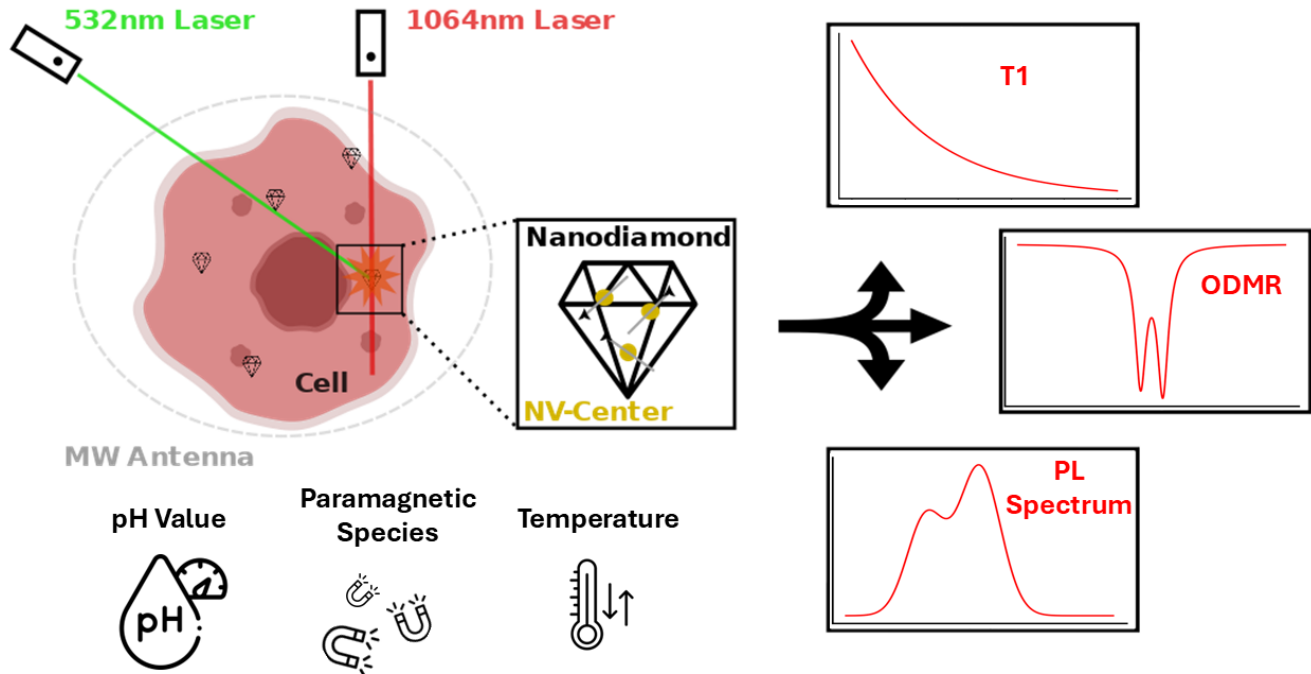


FIG. 1. Graphical abstract illustrating the exploration of effects of NIR laser on NV center for bio-sensing.

ing experimental conditions [4]. We employ a controlled 30 to 60mW NIR laser, with a pulsing sequence inspired by [19], and suggest that the approach can facilitate more precise and reliable intracellular biosensing assessments while keeping any undesirable NIR effect low.

Previous efforts by Aslam et al. [20] have already explored the impact of near-infrared (NIR) laser irradiation on the properties of NV centers, revealing that NIR irradiation can significantly modify NV photoluminescence and enhance spin-lattice relaxation processes, using factors such as NIR laser power (around 30mW) and pulse duration (around 30ns) [21]. The existing literature provides different and sometimes conflicting explanations on the physical mechanisms induced by NIR radiation, which modify both the optical and spin properties of NV centers [9, 14, 15, 21–23].

In our experiment, we first investigated the effect of the NIR laser on the fluorescence of FNDs in two scenarios: dry FNDs and optically trapped FNDs. We then demonstrated the sensing capabilities of the optically trapped FNDs, which included measurements in different pH environments, controlled temperature variations, and the addition of a paramagnetic species (Gd^{3+}). We propose that changes in spin and photoluminescence properties may be due to three effects: i) heating of the FNDs induced directly by NIR laser irradiation of the FNDs by the NIR laser, ii) a charge state recombination and ionization rate that depends on the NIR laser power and iii) a sensitivity effect, where the NIR laser alters the FNDs'

response to their environment [24]. The sensitivity effect is particularly important for those sensing protocols that rely on NV centers positioned close to the surface of the FNDs [4, 17]. For example, the pH of the surrounding environment plays a significant role in the behavior of NV centers in FNDs. Variations in pH can influence the charge state dynamics of NV centers, which in turn affects their fluorescence properties and overall sensitivity in sensing applications [13, 18, 24, 25].

In this article, we build upon existing hypotheses that the effects of NIR irradiation on NV centers involve both heating, as suggested by previous studies [22], and redistribution between charge states [21, 23]. We aim to provide a more comprehensive understanding of these combined effects, thus offering new insights into optimizing optically trapped NV-based sensing protocols [9]. The paper is organized as follows: Section II describes the methods, including sample preparation, the optical setup, FND trapping, and sensing experiments. Section III presents the results, focusing on photoluminescence spectrum analysis, optically detected magnetic resonance measurements, T1 relaxometry, and a combined statistical analysis. Section IV discusses the implications of the findings, including thermal effects, charge state dynamics, and their interplay, along with alternative considerations. Finally, Section V explores the sensing capabilities of trapped FNDs.

II. METHODS

A. Sample Preparation

Fluorescent FNDs with a nominal diameter of 120 nm (Sigma-Aldrich, 798088) were used for most of the experiments reported in this article if not stated otherwise. They possess a significant number of nitrogen-vacancy (NV) centers due to high concentration of 3ppm. To prepare the FND suspension, 1 μL of the commercial stock solution of FNDs was diluted in 300-700 μL of deionized water depending on the desired concentration and before sonicating for 10 minutes. Next, the FND suspension was deposited on a petri dish (Mattek, part no P35G-1.5-10-C.), thoroughly cleaned to remove any contaminants that could interfere with the experiments and plasma ionised in order to make the surface hydrophilic, ensuring an even distribution of FNDs on the surface. Plasma treatment was applied for 30 seconds in a simple custom-device with a closed chamber in PMMA and under ambient conditions in which an electrode (Electro Technic Product, BD-20V) could be positioned close to the petri dish surface. The plasma treatment modifies the surface energy of the petri dish by breaking chemical bonds on the surface and introducing polar functional groups, thereby inducing the hydrophilic state [26]. Approximately 3 μL of the FND suspension was then carefully deposited onto the clean petri dish using a micropipette. The suspension was gently spread across the surface before allowing it to dry. The drying process took place at room temperature to minimize any potential alterations to the FND properties potentially caused by excessive heating or cooling. After the solution had completely evaporated, the sample was ready for the optical experiments described in the following. The preparation of FNDs in the liquid environment also starts with the dilution steps and cleaning of the petri dish, but to maintain the FNDs in solution, the petri dish was not plasma treated and the solution was not left for evaporation.

FNDs with a nominal size of 70 nm were used for sensing experiments as they are preferably used in our most recent cell experiments [27]. The FNDs (Sigma-Aldrich 1003626896) were prepared following the same protocol. A suspension of FNDs was created by diluting 1 μL of the commercial stock solution in 1000 μL of deionized water, followed by sonication for 10 minutes to ensure a homogeneous dispersion. Approximately 500 μL of the suspension was deposited in a Petri dish that was thoroughly cleaned.

B. Optical Setup

The dried FND sample was placed inside a mini-incubator (pecon XS 2000) in an optical setup based on a customized Thorlabs OTKB/M. Customization included a different objective (Nikon, CFI PLAN APO LAMBDA 100x OIL NA 1.45 WD 0.13) and long-distance condenser

lens (Mitutoyo M Plan Apo 10x / 0.26). The setup is constructed around an inverted microscope configuration, equipped with a high-resolution camera (Teledyne Prime 95B), and two lasers for the simultaneous illumination and manipulation of the FNDs. A green laser (Coherent Verdi G5) with a wavelength of 532 nm was utilized for the excitation of the NV centers, enabling the initialization and readout of their spin states. The second laser (Cobolt Rumba, 3W) is operating in the near-infrared (NIR) at a wavelength of 1064 nm and used for FND trapping. This wavelength falls within the biological transparency window, which minimizes absorption and reduces the risk of significant heating effects in biological samples. The two lasers were aligned and their beams combined using a dichroic mirror, ensuring they shared the same optical path before being focused onto the sample through the microscope objective, as detailed in Fig. 2. By trapping an FND and then adjusting the position of the green laser to maximize the signal on the photon counter, we ensured the same focal point for both the green and NIR lasers. Additionally, acousto-optic modulators (AOMs) were used to precisely control the timing and intensity of the laser beams, enabling fine-tuned manipulation of the FNDs.

As illustrated in Fig. 2, several modes of detection were installed: i) camera detection, ii) spectrometer detection and iii) photon count detection. A motorized flip-mirror ensures the ability to rapidly shift between camera detection or either spectrometer or photon count detection. The fluorescence spectrum of the FNDs is recorded and analyzed by a fiber coupled spectrometer (Ocean Optics X00428) while alternatively photon counts are measured with a fiber coupled avalanche photo detector (Excelitas SPCM-AQRH-13-Fc). In addition, to measure the ODMR spectrum of FNDs, an Agilent N5181A signal generator connected to an amplifier (MiniCircuits ZHL-45) is connected to a copper wire antenna placed approximately 1mm above the sample. When the flip-mirror is positioned towards the camera, the latter captures high-resolution images of the FNDs illuminated during the experiments in real time. The combination of different detection methods thus made it possible to continuously monitor the position of the FNDs, determine whether they were isolated or in aggregates, and analyse their photoluminescence properties throughout the experimental process.

C. FND Trapping

For the FND trapping experiments, solution samples were used to ensure the FNDs remained mobile during the experiment.

The NIR laser was utilized for trapping the FNDs in the focused beam [28–31]. For T_1 relaxometry, the temporal sequence of the green and trapping lasers, as illustrated in Fig. 3, is carefully designed to minimize the overlap between the two lasers [19]. This approach re-

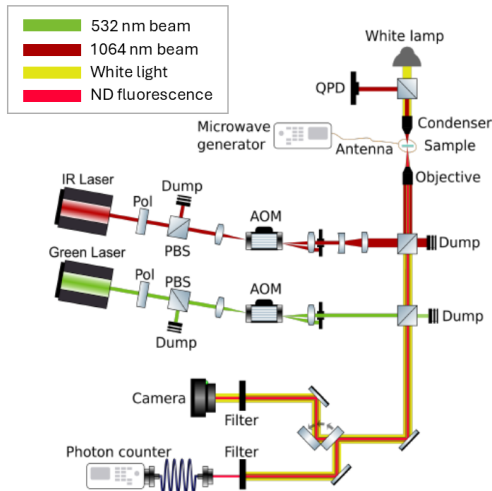


FIG. 2. Illustration of the optical setup with the most important lasers, optical lenses, filters and equipment.

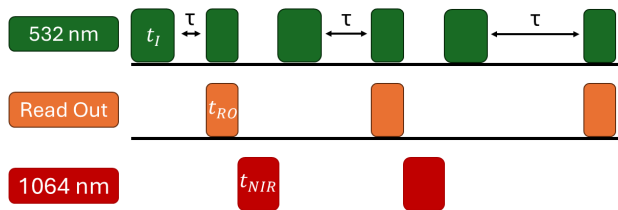


FIG. 3. Laser sequence for T_1 measurement. In green the 532 nm laser and in red the 1064 nm laser. $t_{NIR} = 20\mu s$, $t_I = 35\mu s$, $t_{RO} = 15\mu s$ and τ from $7.2\mu s$ to $720\mu s$.

duces potential spin-mixing effects from the NIR laser, while maintaining the stability of the trap. The green laser was pulsed for $35\mu s$ for the excitation and $15\mu s$ for the readout of the NV center spin states. The NIR laser was pulsed for $20\mu s$ for the trapping of the FNDs. By using this sequence, we optimized the trapping stability during T_1 relaxometry measurement and minimized NIR irradiation potential impact on the measurements.

The sensing experiments utilized the FND trapping protocol described below, and the CW NIR laser power was set to 60 mW to stabilize the FNDs in the optical trap. However, for manipulations involving changes to the surrounding medium, the CW NIR laser power was increased to 100 mW to ensure that the FND remained trapped despite turbulence in the medium. After the modifications, the laser power was reduced back to 60 mW for subsequent measurements.

D. Sensing Experiments

1. Gd^{3+} Magnetic Noise Detection

For the experiments detecting paramagnetic species, a gadolinium solution (0.45 M in acetate) was gradually added to the FND's environment. The concentrations were incrementally adjusted, and measurements were performed after each addition to evaluate the changes in the NV center properties.

2. pH Sensing

For the pH sensing experiments, an initial 0.1 M NaOH(aq) solution at pH 13 was prepared. The pH was then progressively decreased by adding controlled volumes of a 1 M HCl solution. After each pH adjustment, the properties of the NV centers were measured while the FNDs were maintained in the optical trap at 60 mW .

3. Temperature Sensing

For the temperature sensing experiments, the medium containing the FNDs was initially maintained at $37\text{ }^\circ\text{C}$ using an incubator. The temperature was then increased in steps of 1 K , allowing the evaluation of temperature changes on the NV center properties. After each change of the set temperature of the incubator, we waited 10 minutes before the measurements were conducted.

III. RESULTS

We begin by presenting the main results of our experiments, starting with the examination of the general fluorescence properties of NV-centers within the FNDs through Photoluminescence (PL) spectroscopy. This foundational assessment provides an overview of the baseline optical characteristics and helps identify any immediate changes induced by the NIR laser irradiation. Following the PL spectrum analysis, we delve into the variations in fluorescence intensity as a function of optically detected magnetic resonance (ODMR) conditions. This step is crucial for understanding the impact of NIR irradiation on the magnetic resonance properties of the NV centers. Finally, we conduct T_1 -relaxometry to investigate the spin relaxation dynamics, providing a detailed examination of the spin-state populations and their evolution under different NIR laser parameters. This approach from general fluorescence to specific spin dynamics allows for a comprehensive evaluation of the NIR irradiation effects on the NV centers. PL spectrum measurement and ODMR measurement were conducted with CW NIR laser irradiation.

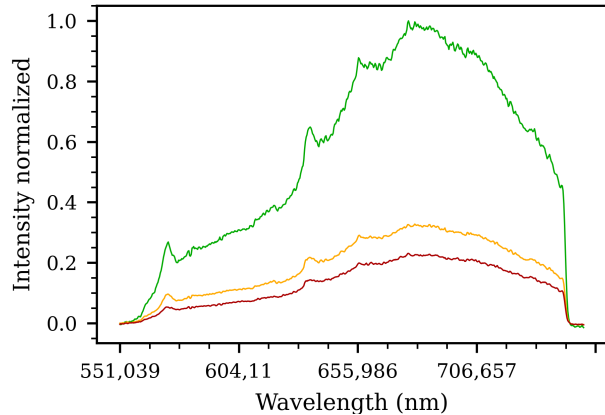


FIG. 4. **Effect of CW NIR laser on dry FND emission spectrum.** Optical emission spectrum of dry FND on glass under CW NIR laser exposure at 0 mW (green), 30 mW (orange) and 60 mW (red) of 1064 nm laser power.

A. Photoluminescence Spectrum Analysis

We conducted PL spectroscopy of FNDs with varying NIR power. The FNDs were either dried on glass substrates or trapped in water to examine the influence of the surrounding medium.

Effect of NIR Laser Power on PL Spectrum Intensity

We exposed single FNDs to CW NIR laser at power levels of 0 mW, 30 mW, and 60 mW and for each power observe the PL spectrum from 550 nm to 750 nm with our spectrometer.

Our PL measurements revealed significant alterations in the spectral intensities of both zero-phonon lines (ZPL) from the two NV charge states upon CW NIR laser exposure. Notably, as a function of NIR laser power there was a slightly more pronounced reduction in the spectral intensity of NV^- compared to NV^0 . As shown in Fig. 4, the ZPL intensity of NV^0 at 575 nm decreased by 29.5% and 32.4%, while the NV^- ZPL intensity at 637 nm decreased by 52.8% and 62.3% when the CW NIR laser power was increased from 0 mW to 30 mW and 60 mW, for the condition with FNDs dry on glass. For the fluorescence spectrum (like Fig. 4), the curves remain quite similar when water is added, although with less effect of increase in NIR laser intensity from 30mW to 60mW (data not shown) and the difference between 30 mW and 60 mW is even more reduced for FNDs that are trapped in water, cf. Fig. 5. Quantitatively, we observe a 1.2% general intensity difference from 30 mW to 60 mW for FNDs on glass with water while the same figure is 0.7% for FNDs trapped in water.

To determine the ratio of NV^0 to NV^- emission intensities under CW NIR laser powers of 0 mW, 30 mW, and 60 mW we integrated the emission intensities over

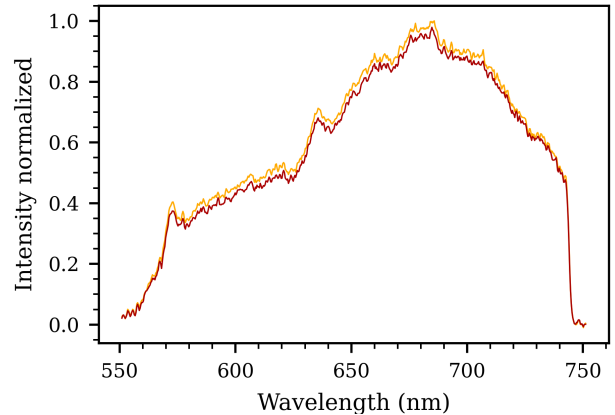


FIG. 5. **Effect of CW NIR laser on trapped FND emission spectrum.** Optical emission spectrum of FND trapped in water CW NIR laser at 30 mW (orange) and 60 mW (red) of 1064 nm laser power.

the respective spectral ranges for NV^0 (550–620 nm) and NV^- (655–750 nm), but compared to the procedure of Ref. [13], we applied a normalization factor to account for the difference in spectral ranges:

$$\frac{NV^0}{NV^-} = \left(\frac{\sum_{\lambda=550}^{620} I_{\lambda}}{\sum_{\lambda=655}^{750} I_{\lambda}} \right) \times \frac{95}{70} \quad (1)$$

We observe that the NV^0/NV^- emission ratio stays the same for trapped FNDs, 0.45 for both 30mW and 60mW NIR laser power. In contrast, it rises from 0.39 without NIR irradiation to 0.51 with 60 mW NIR laser power for dry FND on glass. All results are displayed in Fig. 10.

B. Optically Detected Magnetic Resonance Measurements

We further examined the influence of CW NIR laser power on the ODMR resonance frequency and contrast for FNDs dried on glass substrates and those trapped in water.

Effect of CW NIR Laser Power on the Zero Field Splitting of the NV Center

We exposed the FNDs to CW NIR laser powers of 0 mW, 30 mW, and 60 mW, and measured the resulting ODMR spectra. Our primary observation was a shift in the resonance frequency with increasing CW NIR laser power, as illustrated with an example in Fig. 6.

For FNDs dried on glass substrates, the resonance frequency shifted significantly to the lower frequencies. Specifically, the resonance frequency shift increased in

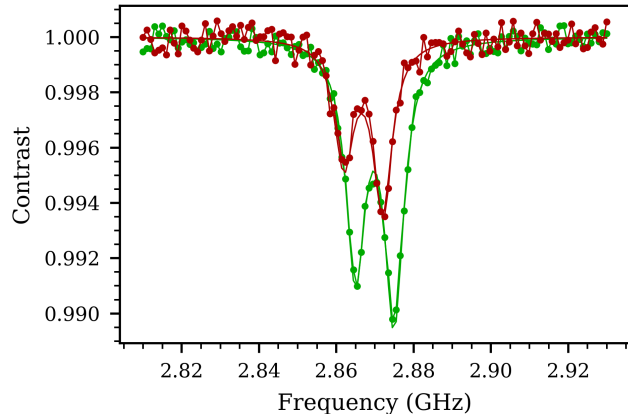


FIG. 6. **Effect of CW NIR laser power on ODMR spectrum of dry FND.** ODMR spectra of dry FNDs under CW NIR laser exposure at 0 mW (green) and 60 mW (red) of 1064 nm laser power. The resonance frequency shift and decrease in contrast with increasing CW NIR power is observed.

absolute value from -0.31 ± 0.54 MHz at 0 mW to -5.83 ± 0.46 MHz at 60 mW of CW NIR power; both values given relative to the expected 2.87 GHz. In contrast, FNDs trapped in water exhibited much smaller frequency shifts, with changes of -0.84 ± 0.21 MHz at 30 mW and -1.58 ± 0.33 MHz at 60 mW (relative to the expected 2.87 GHz). Examples are shown in Fig. 6 and Fig. 7 while combined results are displayed in Fig. 11. As before, for the similar experiment when water was added to the same FND that remained stuck on the glass slide, the ODMR spectra show a trend very similar to Fig. 6 although the difference between 30 mW and 60 mW of NIR power is less pronounced (data not shown).

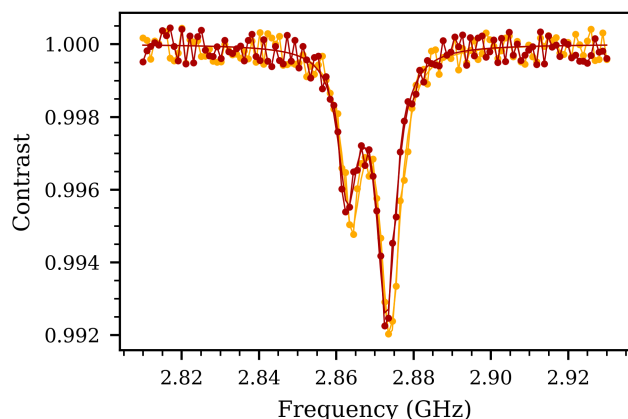


FIG. 7. **Effect of CW NIR laser power on ODMR spectrum of trapped FND.** ODMR spectra of FNDs trapped in water under CW NIR laser exposure at 30 mW (orange) and 60 mW (red) of 1064 nm laser power. The resonance frequency shift and decrease in contrast with increasing CW NIR power is observed.

C. T_1 Relaxometry Measurements

We conducted T_1 relaxometry experiments under different NIR laser power. As above, FNDs were either dried on glass substrates or suspended in water to assess the influence of the surrounding medium on the T_1 relaxometry measurements with NIR irradiation. The samples were exposed to NIR laser powers of 0 mW, 30 mW, and 60 mW, and the corresponding T_1 values were measured. For these experiments, the pulsing sequence in Fig. 3 was applied.

Effect of NIR Laser Power on T_1 Relaxation Times

First, we investigate how the T_1 value of dry FNDs is affected by NIR irradiation. For FNDs dried on glass substrates, we observed a significant decrease in the T_1 relaxation times with increasing NIR laser power. As shown in the example in Fig 8, the mean T_1 value decreased from 241 ± 21 μ s at 0 mW NIR power to 136 ± 19 μ s at 60 mW NIR power. When water was added to the same FND that remained stuck on the glass slide, the T_1 values showed very similar changes. The mean T_1 value decreased from 237 ± 25 μ s at 0 mW NIR power to 154 ± 17 μ s at 30 mW NIR power and 143 ± 21 μ s at 60 mW NIR power. (data not shown).

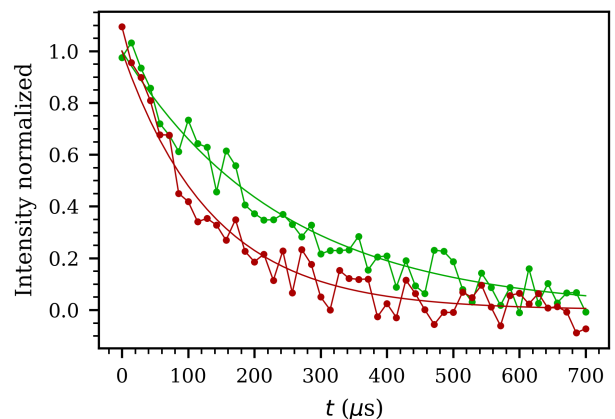


FIG. 8. **Effect of NIR laser power on T_1 relaxation times of dry FNDs.** T_1 relaxometry measurements for FNDs dried on glass under NIR laser powers of 0 mW (green) and 60 mW (red) at 1064 nm wavelength. Pulsing as in Fig 3.

For FNDs trapped in water, the decrease in T_1 due to NIR irradiation was significantly less. As depicted in the example in Fig. 9, we do not observe any significant change in the 2 curves. The T_1 values for trapped FNDs were 179 ± 8 μ s at 30 mW and 176 ± 8 μ s at 60 mW, showing a negligible decrease compared to the values at 0 mW, with all results summarized in Fig. 11.

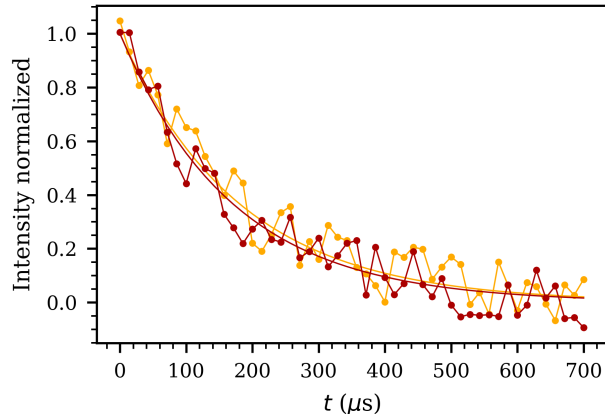


FIG. 9. **Effect of NIR laser power on T_1 relaxation times of trapped FNDs.** T_1 relaxometry measurements for FNDs trapped in water under pulsed NIR laser powers of 30 mW (orange) and 60 mW (red) at 1064 nm wavelength.

D. Combined Statistical Analysis

In this section, we present a comprehensive statistical analysis of our experimental results.

Relationship Between NV^0/NV^- Ratio and ODMR Frequency Shift

Figures 10.a, 10.c, 11.a and 11.b illustrate the dependence of the NV^0/NV^- fluorescence intensity ratio and the ODMR resonance frequency shift for FNDs under varying CW NIR laser powers.

For FNDs dried on glass substrates, we observe a significant increase in the NV^0/NV^- fluorescence intensity ratio and a corresponding shift in the ODMR resonance frequency with increasing CW NIR power from 0 mW to 60 mW.

In contrast, for FNDs trapped in water, the NV^0/NV^- fluorescence intensity ratio and ODMR frequency shift exhibit much smaller changes with increasing CW NIR power. This suggests that the aqueous environment mitigates the effects of CW NIR irradiation.

Correlation Between T_1 Relaxation Times and ODMR Frequency Shift

Figures 10.b, 10.d, 11.a and 11.c show the relationship between the T_1 relaxation times and the ODMR resonance frequency shift for FNDs under varying NIR laser powers. T_1 was obtained with the pulse sequence as in Fig 3 while the ODMR was obtained with CW NIR irradiation.

For FNDs dried on glass substrates, there is an effect between T_1 times and ODMR frequency shifts with increasing NIR power. The significant decrease in T_1 times

and increase in frequency shift suggest that NIR irradiation enhances spin relaxation processes.

For FNDs trapped in water, the T_1 relaxation times remain relatively constant, and the ODMR frequency shifts exhibit minimal changes with increasing NIR power.

Overall, the data suggest that the aqueous environment reduces the effect of NIR irradiation on ODMR-frequency shifts. Further, our results confirm that with specific NIR irradiation sequences and optimizing laser parameters, cf. Fig. 3 and Ref. [19], potential detrimental effects of NIR on T_1 relaxation can be significantly mitigated, even with FNDs dry on glass.

Statistical Analysis Using ANOVA

To study the significance of the observed effects, we performed an Analysis of Variance (ANOVA) test on the T_1 relaxation times, ODMR frequency shifts, and NV^0/NV^- fluorescence intensity ratios. The ANOVA results are summarized in Table I.

TABLE I. **ANOVA test results for the effect of NIR laser power on FNDs dried on glass substrates, on glass after adding water and trapped in water.** The p-values indicate the significance of differences observed across NIR power levels for T_1 relaxation times, ODMR frequency shifts, and NV^0/NV^- ratios.

	p-value
FNDs dried on glass	
T_1 Relaxation Time	< 0.0001
ODMR Frequency Shift	< 0.0001
NV^0/NV^- Ratio	0.0024
FNDs on glass with water	
T_1 Relaxation Time	0.072
ODMR Frequency Shift	0.008
NV^0/NV^- Ratio	0.201
FNDs Trapped in Water	
T_1 Relaxation Time	0.221
ODMR Frequency Shift	0.073
NV^0/NV^- Ratio	0.371

For FNDs dried on glass substrates, the very low p-values ($p < 0.01$) for all three parameters confirm that the differences observed with varying NIR laser powers are statistically significant. This indicates that NIR irradiation has a considerable impact on the NV centers' properties in air.

For FNDs on glass substrates after adding water, the medium p-values ($0.01 < p < 0.2$) for all three parameters confirm that the differences observed with varying NIR laser powers are not always statistically significant. In fact, the difference between no NIR laser and NIR laser is significant but the differences between 30 mW and 60 mW power of NIR laser are not significant.

In contrast, for FNDs trapped in water, the p-values are high ($p > 0.07$), suggesting that the differences observed across different NIR power levels are not statisti-

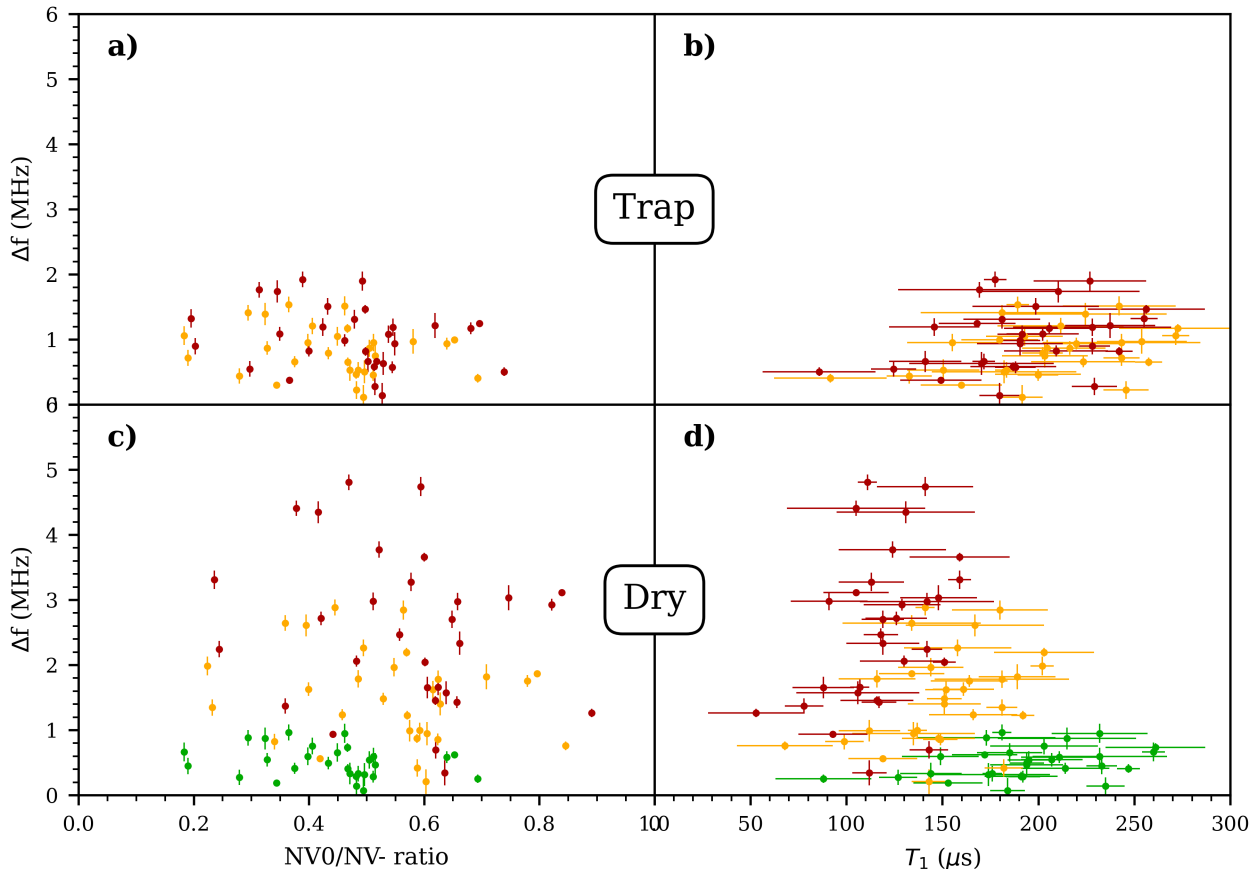


FIG. 10. a) Correlation between NIR laser power, ODMR resonance frequency shift and NV^0/NV^- fluorescence intensity ratio for FNDs trapped inside water. b) Correlation between NIR laser power, ODMR resonance frequency shift and T_1 -relaxometry times for FNDs trapped inside water. c) Correlation between NIR laser power, ODMR resonance frequency shift and NV^0/NV^- fluorescence intensity ratio for FNDs dry on glass. d) Correlation between NIR laser power, ODMR resonance frequency shift and T_1 -relaxometry times for FNDs dry on glass. Data for 30 FNDs exposed to 0 mW (green), 30 mW (orange), and 60 mW (red) of 1064 nm NIR laser irradiation. CW NIR for ODMR and spectra, pulsed NIR as in Fig 3 for T_1 -relaxometry. In general, we observe what appears to be a trend with differences between the three powers of NIR laser light for FNDs dry on glass, and no such trend for FNDs in the optical trap in water.

cally significant. This reinforces the conclusion that the aqueous environment mitigates the effects of NIR irradiation on the NV centers.

E. Charge State Dynamics

To understand and quantitatively model the effects of NIR laser illumination on the charge state dynamics and fluorescence properties of NV centers in FNDs, we investigate a comprehensive rate equation model [32]. This model accounts for the various optical transitions, inter-system crossings, ionization, and recombination processes that occur when NV centers are simultaneously exposed to green and NIR laser excitation.

The NV center can exist in two charge states: the negatively charged NV^- and the neutrally charged NV^0 .

Each charge state has its own ground and excited electronic states, as well as inter-system crossing pathways to metastable singlet states. The model considers 8 states as illustrated in the schematic energy level diagram in Fig. 12.

The population dynamics of the NV centers are described by a set of coupled differential equations representing the rates of change of the population probabilities P_i in each state [32]. The rates of change had to be adapted to our experimentation with green 532 nm and NIR 1064 nm laser.

The model is based on the following assumptions:

- **Steady-State Approximation:** The populations reach a steady state within the simulation time, allowing us to analyze the equilibrium behavior.
- **Neglect of Higher-Order Processes:** Multi-

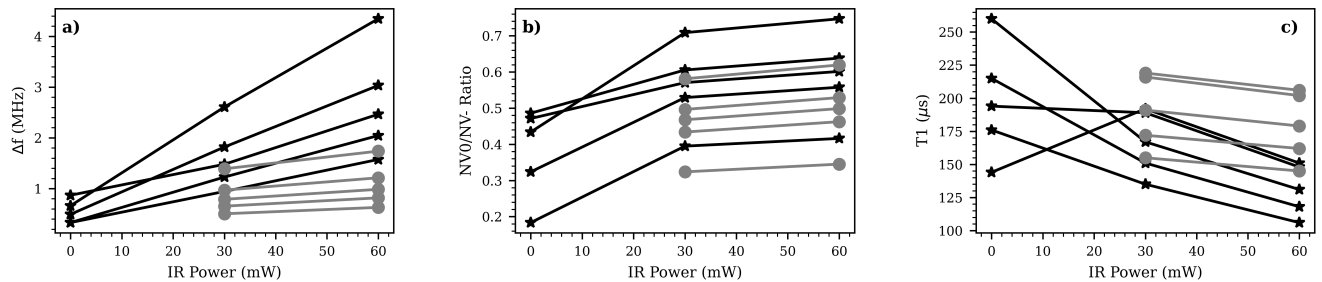


FIG. 11. Summary of experimental results, showing variation for individual nanodiamonds. (a) ODMR resonance frequency shift, (b) NV^0/NV^- fluorescence intensity ratio, and (c) T_1 relaxometry times as functions of NIR laser power. Data for 5 random FNDs dry on glass (black stars) and trapped in water (gray circles) with 1064 nm NIR laser irradiation.

photon processes and higher excited states are neglected due to their low probabilities under the experimental conditions.

- **Constant Rate Coefficients:** The rate coefficients are assumed to be constant and independent of the local temperature and environmental factors.
- **No External Fields:** Effects of external magnetic or electric fields on the transition rates are not included.

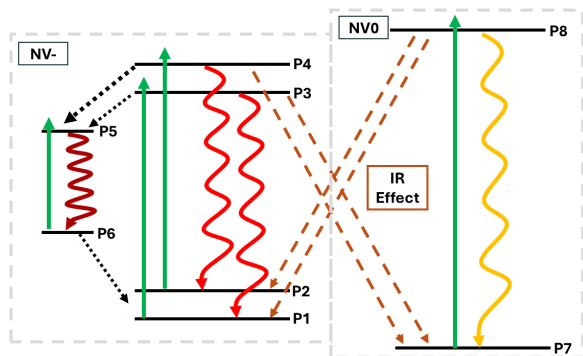


FIG. 12. Energy level diagram of the NV center, showing the ground states (P1, P2 and P7), excited states (P3, P4 and P8), singlet states (P5 and P6), and the transitions between them. Solid arrows represent radiative transitions, dotted arrows represent non-radiative transitions, and dashed arrows represent ionization and recombination processes.

Population Dynamics of NV^- and NV^0 Centers

The simulation results reveal that at low CW NIR laser powers, the population of NV^- centers increases slightly, while the NV^0 population decreases. This is attributed to enhanced recombination processes facilitated by the NIR photons, which convert NV^0 centers back to NV^- . Specifically, up to an CW NIR power of approximately

10 mW, the NV^- population increases by about 8% compared to the case without CW NIR illumination.

However, as the CW NIR power increases beyond this threshold, the trend reverses. The NV^- population begins to decrease, and the NV^0 population increases. At a CW NIR power of 60 mW, the NV^- population decreases by approximately 10% from its maximum value, while the NV^0 population increases correspondingly. This inversion is due to the saturation of recombination processes and the dominance of ionization processes at higher CW NIR powers, which ionize NV^- centers back to NV^0 . The threshold depends on the recombination rate, ionization rate and on the initial population of each state.

Fluorescence Intensity and NV^0/NV^- Ratio

The total fluorescence intensity from the NV centers decreases with increasing CW NIR power (Fig. 13). This decrease is primarily due to the reduced population of NV^- centers and the lower fluorescence quantum yield of NV^0 centers. The fluorescence from NV^- centers dominates the emission under low CW NIR power, but as the CW NIR power increases, the contribution from NV^0 centers becomes more significant and we observe a saturation in the fluorescence.

The ratio of NV^0 to NV^- fluorescence intensities (F_{NV^0}/F_{NV^-}) increases with CW NIR power. At low CW NIR powers, this ratio is low due to the predominance of NV^- fluorescence. As the CW NIR power increases, the ratio rises slowly, indicating a relative increase in NV^0 emission. This change in the fluorescence ratio affects the overall spectral characteristics and can influence the detection sensitivity in applications relying on NV^- fluorescence.

Consistency with Experimental Observations

The trends observed in the simulation align with the experimental results. The initial increase and subsequent decrease of the NV^- population with increasing

NIR power explain the non-monotonic behavior of fluorescence intensity and NV^0/NV^- fluorescence intensity ratio observed experimentally. The simulation provides a quantitative framework to understand how NIR illumination influences the charge state dynamics and, consequently, the optical and spin properties of NV centers.

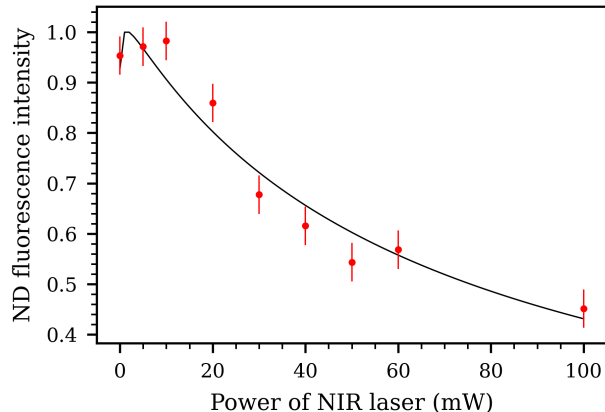


FIG. 13. Total fluorescence intensity from NV centers as a function of NIR laser power. (Black: Theory, Red: Experimental observations).

F. Temperature Simulation

To model the temperature increase induced by the NIR laser on FNDs, we simulated the heat transfer. The simulation accounts for the absorption of laser energy by the FND and the subsequent heat dissipation into the surrounding medium (water or air). The key processes considered are:

1. **Energy Absorption:** The FND absorbs a portion of the incident laser power, leading to an increase in its internal energy and temperature.
2. **Heat Loss:** Heat is lost from the FND to the surrounding medium through conduction and convection, depending on the thermal properties of the medium.

The simulation is based on the following assumptions:

- **Uniform Temperature Distribution:** The FND is assumed to have a uniform temperature at any given time due to its small size.
- **Negligible Radiation Losses:** Heat loss due to thermal radiation is neglected because it is insignificant compared to conduction at the temperatures considered.
- **Constant Thermal Properties:** The thermal properties of the FND and the medium are assumed constant over the temperature range studied.

- **Steady-State Heat Transfer Coefficient:** The convective heat transfer coefficient h is considered constant and based on the thermal conductivity of the medium.
- **No Phase Change:** The medium remains in the same phase (liquid for water, gas for air) throughout the simulation.

Temperature Evolution During a 500 ns NIR Pulse

The simulation modeled the temperature change of an FND during a 500 nanosecond NIR laser pulse followed by a cooling period after the laser is turned off. The results show that the FND's temperature increases during the laser pulse and decreases afterward, illustrating the transient thermal response to short laser excitation. In our sequence the NIR pulse was longer ($20\mu s$), in the simulation the choice of 500 ns has been done to show the temperature increase before saturation; we observe saturation after 75 ns for the FND in air and 435 ns for the FND in water.

In Water: The temperature increase of the FND is minimal due to the high thermal conductivity and heat capacity of water. The simulation indicates that during the 500 ns NIR pulse:

- The maximum temperature rise (ΔT_{\max}) is approximately 2 K above the ambient temperature.
- The temperature increases steadily during the laser pulse and rapidly returns to ambient temperature within nanoseconds after the laser is turned off.

In Air: The temperature increase is more pronounced because air has lower thermal conductivity and heat capacity. The simulation results show:

- The maximum temperature rise reaches approximately 41 K above the ambient temperature during the 500 ns NIR pulse.
- The temperature increases during the laser pulse and decreases more slowly than in water after the laser is turned off.

Consistency with Experimental Observations

The simulation results align with experimental observations where pulsed NIR illumination causes negligible thermal effects in aqueous environments. This supports the conclusion that charge state dynamics are the primary mechanism affecting NV center behavior under short NIR pulses in water.

In experiments conducted in air, temperature increases contribute to shifts in ODMR frequency and should be

accounted for. These shifts correspond to a 2 MHz shift in the ODMR resonance frequency which is what we experimentally observe.

IV. DISCUSSION: EFFECTS OF NIR LIGHT ON FNDs

Our experimental and simulation results reveal a complex interplay between thermal dynamics and charge state transitions in NV within FNDs under NIR illumination. The observed effects include a decrease in total fluorescence intensity, reduction in spin-lattice relaxation time, shift in the ODMR resonance frequency, decrease in ODMR contrast, and an increase in the NV^0/NV^- fluorescence ratio.

A. Thermal Effects Induced by NIR Illumination

One primary mechanism contributing to these observations is the localized heating induced by the NIR laser. The shift in the ODMR resonance frequency with increasing NIR power, as shown in Figures 6, 7 and 10, and 11a), suggests an increase in temperature within the FNDs. This is consistent with the known temperature dependence of the zero-field splitting parameter D of the NV center, which decreases with increasing temperature at a rate of approximately -74 kHz/K [33, 34].

However, the extent of the thermal effect is significantly influenced by the surrounding medium's thermal properties. Media with higher thermal conductivity and heat capacity, such as water, dissipate heat more efficiently than air, resulting in smaller temperature increases in the FNDs. This is supported by our temperature simulations, which show minimal temperature rise in water compared to air during NIR illumination. Consequently, FNDs trapped in water exhibit much smaller ODMR frequency shifts and negligible changes in T_1 times with increasing NIR power, as shown in Figures 7, 10 and 11.

B. Charge State Dynamics and Fluorescence Changes

In addition to thermal effects, the NIR laser alters the charge state dynamics of the NV centers. Our simulations of charge state dynamics indicate that at low NIR power levels, there is a slight increase in the NV^- population due to enhanced recombination processes facilitated by NIR photons. However, as the NIR power increases beyond a threshold (approximately 10 mW with our parameters), the NV^- population begins to decrease while the NV^0 population increases. This inversion is attributed to the saturation of recombination processes and increased ionization rates at higher NIR powers.

These changes in charge state populations directly affect the fluorescence properties of the FNDs. The total fluorescence intensity decreases with increasing NIR power, as shown in Figure 13. This decrease can be explained by the reduced NV^- population and the lower fluorescence quantum yield of NV^0 centers [35]. The increase in the NV^0/NV^- fluorescence ratio with higher NIR power, depicted in Figures 10 and 11, further confirms the shift in charge state distribution.

Additionally, the increased NV^0 background fluorescence dilutes the ODMR contrast since NV^0 centers do not exhibit spin-dependent fluorescence variations. This is reflected in the decreased ODMR contrast observed in our measurements (Figures 6-7). Charge-state fluctuations also introduce additional pathways for spin relaxation, contributing to the reduction in T_1 times [20, 36].

C. Interplay Between Thermal Effects and Charge State Dynamics

Although both thermal effects and charge state dynamics significantly impact the properties of the NV centers under NIR illumination, their relative contributions depend on the environmental conditions. In FNDs dried on glass substrates, the pronounced ODMR frequency shifts suggest that thermal effects dominate due to inefficient heat dissipation in air.

In contrast, for FNDs trapped in water, the minimal temperature increase reduces thermal effects, making charge-state dynamics more prominent in influencing the NV centers' behavior. The increase in the NV^0/NV^- ratio and the decrease of T_1 -relaxometry times with NIR power without significant ODMR frequency shifts (Figure 10) indicates that charge state transitions are the primary mechanism affecting the fluorescence and spin properties in aqueous environments.

D. Alternative Explanations and Considerations

Although thermal effects and charge state dynamics provide a comprehensive explanation for our observations, alternative mechanisms should be considered. Multi-photon absorption processes could directly excite the NV centers without significant heating. However, the relationship between ODMR frequency shift and NIR power (Figures 7 and 10) supports the thermal interpretation in our experiments.

Moreover, the significant differences in the effects of NIR irradiation between FNDs in air and water emphasize the critical role of the surrounding medium. The statistical analysis using ANOVA (Table I) confirms that the differences observed in FNDs dried on glass are statistically significant, whereas those in FNDs trapped in water are not, reinforcing the influence of environmental thermal properties.

V. SENSING CAPABILITIES OF TRAPPED FNDs

As a final step in the comprehensive investigations, this section explores the potential of optically trapped FNDs with NV centers for sensing applications. Experiments focused on three key parameters: Gd^{3+} concentration, pH, and temperature. Measurements included ODMR, T_1 relaxation, and optical spectrum analysis under variation of the three parameters mentioned above.

A. pH Sensing

The impact of environmental pH on the properties of NV centers was evaluated using buffer solutions with pH values of 1, 7, and 13.

- **T_1 Relaxation:** A decrease in T_1 values was observed as pH increased, indicating a dependence on surface protonation dynamics (Fig. 14.h). This is consistent with reports that high pH conditions stabilize spin relaxation dynamics [1].
- **Optical Spectrum:** A decrease in the NV^0/NV^- fluorescence intensity ratio with increasing pH (Fig. 14.e and 15) suggests that alkaline conditions favor the NV^- charge state, possibly due to deprotonation of surface functional groups, which enhances negative surface potential [37]. The difference in ratio change between FNDs dry on glass without an NIR laser and FNDs trapped with a 60 mW CW IR laser shows a clear advantage of using FNDs in suspension for sensing.
- **ODMR:** No significant changes in resonance frequency (Fig. 14.b) were detected across the tested pH range, indicating minimal impact of pH on electronic spin states.

The NV^0/NV^- fluorescence intensity ratio's dependence on pH underscores the importance of surface chemistry in modulating charge state dynamics, especially with FNDs in suspension.

B. Paramagnetic Species Sensing

The sensitivity of NV centers to paramagnetic gadolinium ions (Gd^{3+}) was investigated through measurements at 3 different values of the concentration.

- **T_1 Relaxation:** A significant decrease in T_1 values was observed with increasing Gd^{3+} concentration (Fig. 14.g). This result aligns with the quenching effect of paramagnetic ions, which enhance spin-lattice relaxation by introducing magnetic noise to the local environment [38].

- **Optical Spectrum:** A decrease in the NV^0/NV^- fluorescence intensity ratio was observed (Fig. 14.d and 16). This can be attributed to charge state dynamics, where Gd^{3+} ions interact with the FND surface, altering the local electrochemical potential and promoting ionization of NV^- to NV^0 [39]. The difference in ratio change between FNDs dry on glass without an NIR laser and FNDs trapped with a 60 mW CW IR laser shows a clear advantage of using FNDs in suspension for sensing.
- **ODMR:** No significant shifts or changes in resonance frequency were detected, suggesting limited interaction between Gd^{3+} ions and the electronic spin states of the NV centers under the tested conditions (Fig. 14.a).

These findings demonstrate the potential of NV centers for detecting paramagnetic species like Gd^{3+} . The sensitivity saturates at higher concentrations due to the finite interaction volume and saturation of surface sites for Gd^{3+} binding. The T_1 -relaxometry provides a robust method for quantifying Gd^{3+} in biological and environmental contexts. However, the effect on charge state dynamics also imply that conclusions from T_1 -relaxometry in otherwise uncharacterized environments should be made with caution, and at best complemented with fluorescence spectrometry. For completeness, we observe that by adding Gd^{3+} to a concentration of 0.1 M, the pH value in the solution increases slightly (by of order 1-2 pH units) which is consistent with our previous observations on the effect of pH on the fluorescence of FNDs..

C. Temperature Sensing

The temperature response of NV centers was evaluated under three conditions: FNDs on glass substrates with no NIR laser irradiation, trapped FNDs with no temperature increase, and trapped FNDs with temperature increases of +1 K and +2 K.

- **ODMR:** A temperature-dependent shift in the resonance frequency was observed, with lower frequencies at higher temperatures (Fig. 14.c). This shift is attributed to the well-known temperature dependence of the NV center's zero-field splitting parameter D , which decreases at a rate of approximately -74 kHz/K [40].
- **T_1 Relaxation:** No significant changes were detected in T_1 values, indicating that spin-lattice relaxation is relatively insensitive to temperature variations within the tested range (Fig. 14.i).
- **Optical Spectrum:** No significant changes in the NV^0/NV^- fluorescence intensity ratio were observed with temperature, suggesting that charge

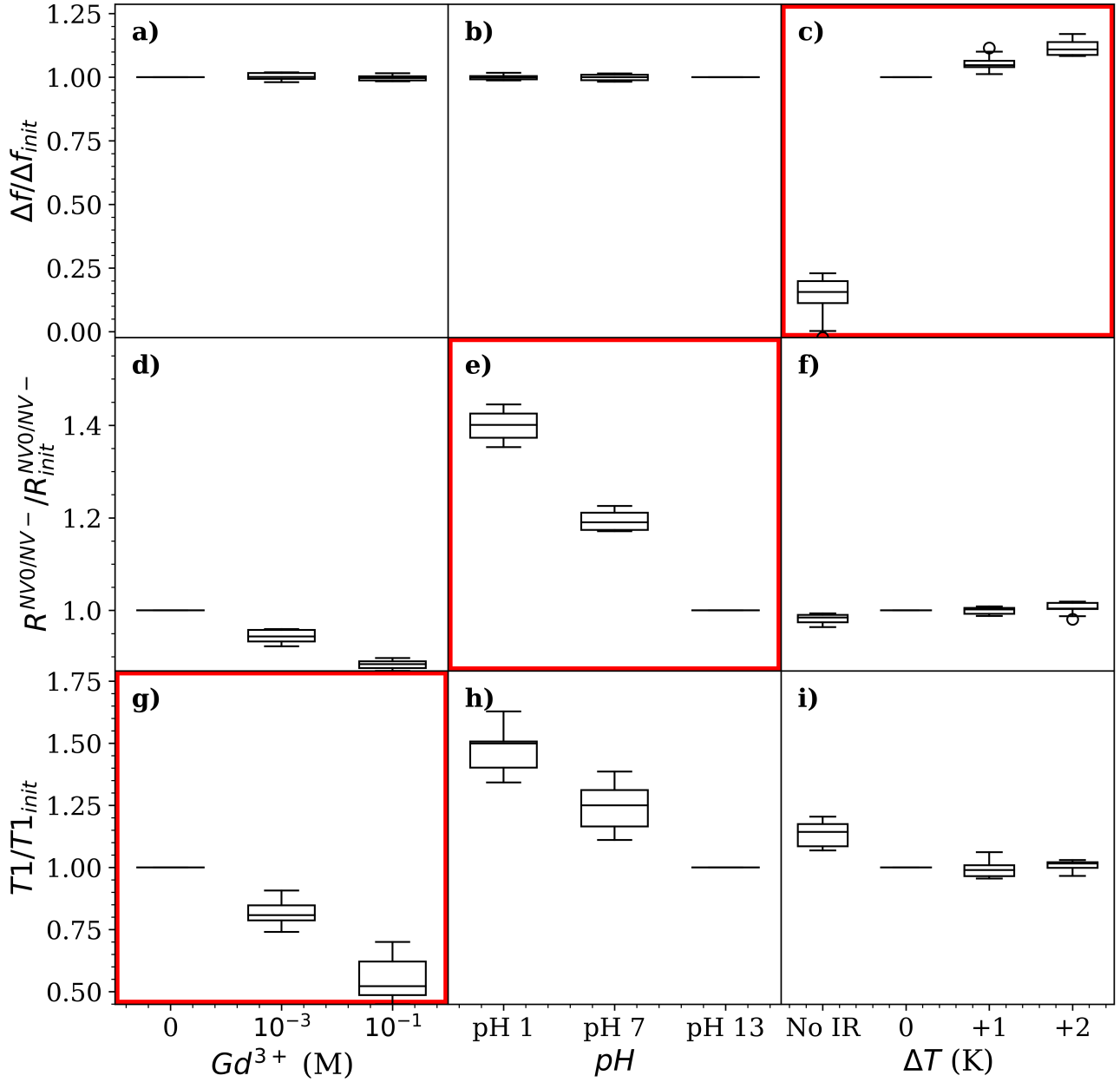


FIG. 14. Variation in three sensing parameters when subject to controlled variation of paramagnetic species, pH, and temperature. a) ODMR resonance frequency shift VS Gd^{3+} concentration. b) ODMR resonance frequency shift VS pH value. c) ODMR resonance frequency shift VS Temperature increase. d) T_1 -relaxometry time VS Gd^{3+} concentration. e) T_1 -relaxometry time VS pH value. f) T_1 -relaxometry time VS Temperature increase. g) NV^0/NV^- fluorescence intensity ratio VS Gd^{3+} concentration. h) NV^0/NV^- fluorescence intensity ratio VS pH value. i) NV^0/NV^- fluorescence intensity ratio VS Temperature increase. The boxplot represent results for 10 FNDs that were trapped for each condition with 60 mW 1064 nm CW NIR laser. In each case, results for Gd^{3+} 0M, pH 13 and 0K trapped were used as reference values for the individual FNDs. The red squares emphasize the optimal measurement method for each sensing parameter. The ODMR resonance frequency value is given relative to the expected 2.87 GHz.

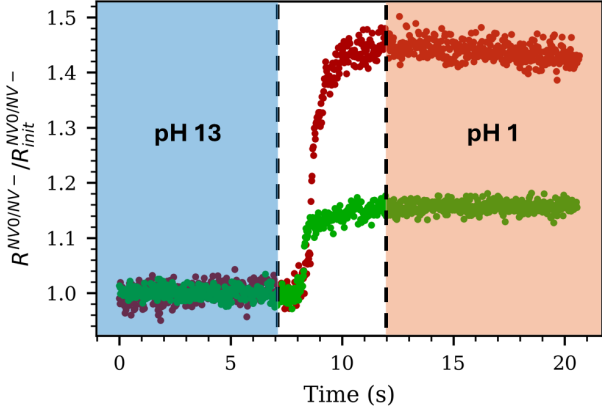


FIG. 15. NV^0/NV^- fluorescence intensity ratio during pH value changes. Measurement of the same FND while changing from pH13 to pH1 by adding HCl solution (Red: FND trapped with 60 mW 1064 nm CW NIR laser, Green: FND on glass without NIR laser).

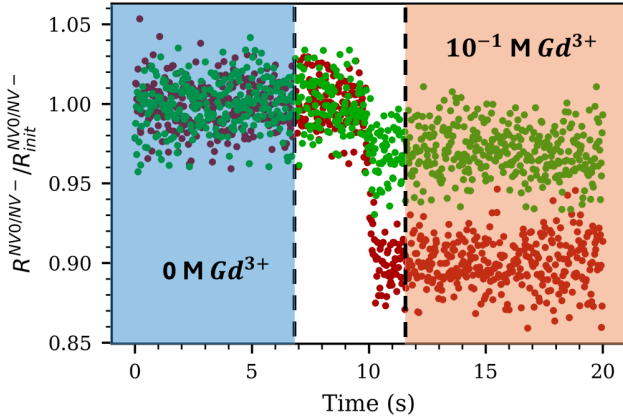


FIG. 16. NV^0/NV^- fluorescence intensity ratio during gadolinium concentration changes. Measurement of the same FND while changing gadolinium concentration from 0M to 0.1M by adding a gadolinium solution (0.45 M in acetate) (Red: FND trapped with 60 mW 1064 nm CW NIR laser, Green: FND on glass without NIR laser).

state dynamics are minimally affected by thermal fluctuations (Fig. 14.f).

ODMR’s temperature sensitivity highlights its utility for high-resolution nanoscale thermometry. The absence of significant T_1 or optical spectral changes simplifies calibration, making ODMR a standalone method for temperature measurements

VI. CONCLUSION

This work investigates the effects of near-infrared (NIR) laser irradiation on fluorescent nanodiamonds

(FNDs) containing nitrogen-vacancy (NV) centers, offering a comprehensive understanding of the interplay between thermal effects, charge state dynamics, and their combined influence on sensing capabilities. By employing an integrated experimental approach combining photoluminescence spectroscopy, optically detected magnetic resonance (ODMR), and T_1 relaxometry, this study elucidates how varying NIR laser powers impact the fluorescence, spin properties, and stability of NV centers in diverse environmental conditions.

A key finding is the dual role of NIR irradiation: in dry environments, thermal effects dominate, resulting in significant shifts in ODMR frequencies and reductions in T_1 relaxation times due to localized heating. In contrast, for FNDs that are fully submerged in aqueous environments, the surrounding water appears to mitigate these thermal effects through efficient heat dissipation, allowing charge state dynamics to take precedence. The increased NV^- , NV^0 fluorescence intensity ratio and its implications for sensing applications underscore the critical role of the surrounding medium in tailoring NV center behavior. The study also demonstrates the sensitivity of optically trapped FNDs to pH variations, temperature fluctuations, and paramagnetic species, establishing these nanodiamonds as versatile tools for nanoscale sensing.

The results have profound implications for the development of robust NV-based sensing protocols. The findings indicate that optimizing NIR laser parameters, including power levels and pulsing sequences, can significantly enhance sensor performance while minimizing adverse effects such as fluorescence quenching and spin relaxation. Additionally, the demonstrated ability to detect and differentiate environmental factors such as pH and gadolinium ions highlights the potential of NV centers for applications in biological sensing and environmental monitoring.

However, this study also reveals critical uncertainties and challenges that must be addressed to fully exploit the potential of NV-based FNDs. Long-term stability under extended NIR irradiation remains an open question, particularly regarding potential degradation of fluorescence and spin properties. The effects of complex biological environments, including interactions with proteins, ions, and other cellular components, are yet to be fully understood. The role of surface functionalization in enhancing NV center stability and sensing accuracy requires further exploration, as does the potential for alternative NIR wavelengths or advanced laser modulation techniques to improve performance.

Theoretical modeling, while providing valuable insights into charge state dynamics and thermal effects, must be expanded to include the complexities of real-world applications. Future work could explore the integration of complementary sensing techniques, such as fluorescence lifetime imaging or advanced magnetic resonance methods, to provide a more holistic understanding of NV center behavior under varying conditions. Fur-

thermore, efforts to miniaturize and automate the experimental setup, enabling *in vivo* applications, would be a critical step toward translating this research into practical diagnostic tools.

In conclusion, this study lays a strong foundation for the continued development of NV-based sensing technologies, bridging fundamental insights with application-driven innovations. By addressing the remaining uncertainties and refining experimental protocols, FNDs with NV centers have the potential to become transformative tools in nanoscale sensing, advancing fields ranging from cellular biology to nanoscale physics.

ACKNOWLEDGMENTS

This work was supported by the Independent Research Fund Denmark (grant no. 0135-00142B) and the Novo Nordisk Foundation (grant no. NNF20OC0061673). We acknowledge discussions with Maabur Sow and Fedor Jelezko, supported by ERC through HyperQ Project (SyG 856432). We further acknowledge insights provided through the student project work of Kristian Lambertsen and Nicolai Kongstad, including the sketch of the experimental setup, Fig. 2.

APPENDIX

As a varying range of values for the rate constants used in the numerical model exist in literature [23, 32], we provide the values used in the simulations presented here.

-
- [1] R. Schirhagl, K. Chang, M. Loretz, and C. L. Degen, Nitrogen-vacancy centers in diamond: Nanoscale sensors for physics and biology, *Annual Review of Physical Chemistry* **65**, 83 (2014).
- [2] Y. Liu, Z. Gu, L. Li, A. Doughty, Y. Li, and X. Zhao, Nanodiamond for biophysical and biomedical applications, *Journal of Materials Chemistry B* **9**, 5402 (2021).
- [3] M. W. Doherty, N. B. Manson, P. Delaney, F. Jelezko, J. Wrachtrup, and L. C. Hollenberg, The nitrogen-vacancy colour centre in diamond, *Physics Reports* **528**, 10.1016/j.physrep.2013.02.001 (2013).
- [4] L. Rondin, G. Dantelle, A. Slablab, F. Grosshans, F. Treussart, P. Bergonzo, S. Perruchas, T. Gacoin, M. Chaigneau, H.-C. Chang, V. Jacques, and J.-F. Roch, Surface-induced charge state conversion of nitrogen-vacancy defects in nanodiamonds, *Phys. Rev. B* **82**, 115449 (2010).
- [5] J. Maze, P. Stanwix, J. Hodges, S. Hong, J. Taylor, P. Cappellaro, L. Jiang, M. Dutt, E. Togan, A. Zibrov, *et al.*, Nanoscale magnetic sensing with an individual electronic spin in diamond, *Nature* **455**, 644 (2008).
- [6] F. Dolde, H. Fedder, M. W. Doherty, T. Nöbauer, F. Rempp, G. Balasubramanian, T. Wolf, F. Reinhard, L. C. Hollenberg, F. Jelezko, *et al.*, Electric-field sensing using single diamond spins, *Nature Physics* **7**, 459 (2011).
- [7] F. Jelezko, T. Gaebel, I. Popa, A. Gruber, and J. Wrachtrup, Observation of coherent oscillations in a single electron spin, *Physical Review Letters* **92**, 10.1103/PhysRevLett.92.076401 (2004).
- [8] L. Childress and R. Hanson, Coherent dynamics of coupled electron and nuclear spin qubits in diamond, *MRS Bulletin* **38**, 134 (2013).
- [9] L. P. Neukirch, J. Gieseler, R. Quidant, L. Novotny, and A. Nick Vamivakas, Observation of nitrogen vacancy photoluminescence from an optically levitated nanodiamond, *Optics Letters* **38**, 2976 (2013), arXiv:1305.1515.
- [10] K. Svoboda and S. M. Block, Biological applications of optical forces, *Annual review of biophysics and biomolecular structure* **23**, 247 (1994).
- [11] F. P. Martinez, A. C. Nuntanara, M. Chipaux, S. K. Padamati, and R. Schirhagl, Nanodiamond relaxometry-based detection of free-radical species when produced in chemical reactions in biologically relevant conditions, *ACS Sensors* 10.1021/acssensors.0c01037 (2020).
- [12] S. Steinert, F. Ziem, L. T. Hall, A. Zappe, M. Schweikert, B. Götz, A. Aird, G. Balasubramanian, L. C. Hollenberg, and J. Wrachtrup, Magnetic spin imaging under ambient conditions with sub-cellular resolution, *Nature Communications* **4**, 1607 (2013).
- [13] M. Sow, H. Steuer, S. Adekanye, L. Ginés, S. Mandal, B. Gilboa, O. A. Williams, J. M. Smith, and A. N. Kapanidis, High-throughput nitrogen-vacancy center imaging for nanodiamond photophysical characterization and ph nanosensing, *Nanoscale* **12**, 21821 (2020).
- [14] G. Balasubramanian, I. Chan, R. Kolesov, M. Al-Hmoud, J. Tisler, C. Shin, C. Kim, A. Wojcik, P. R. Hemmer, A. Krueger, *et al.*, Nanoscale imaging magnetometry with diamond spins under ambient conditions, *Nature* **455**, 648 (2008).
- [15] M. Geiselmann, R. Marty, F. Javier García De Abajo, and R. Quidant, Fast optical modulation of the fluorescence from a single nitrogen-vacancy centre, *Nature Physics* **9**, 785 (2013).
- [16] A. Collins and H. Kanda, Luminescence lifetime of the 1.945 eV centre in type Ib diamond, *Philosophical Magazine B* **48**, 341 (1983).
- [17] A. Gruber, A. Dräbenstedt, C. Tietz, L. Fleury, J. Wrachtrup, and C. von Borczyskowski, Scanning confocal optical microscopy and magnetic resonance on single defect centers, *Science* **276**, 2012 (1997).
- [18] L. Hall, C. Hill, J. Cole, B. Stadler, F. Caruso, P. Mulvaney, J. Wrachtrup, and L. C. Hollenberg, Detection of nanoscale electron spin resonance spectra demonstrated using nitrogen-vacancy centre spins in diamond, *Nature Communications* **7**, 10211 (2016).

TABLE II. Parameters used in the simulation

Parameter	Value	Units	Description
$K_{NV^-}^{(e)}$	27	$(\mu\text{s})^{-1}/\text{mW}$	NV^- excitation rate
$K_{NV^0}^{(e)}$	18	$(\mu\text{s})^{-1}/\text{mW}$	NV^0 excitation rate
τ_{NV^-}	12×10^{-3}	μs	Excited-state lifetime (12 ns)
τ_{NV^0}	20×10^{-3}	μs	Excited-state lifetime (20 ns)
$K_{NV^-}^{(f)}$	$1/\tau_{NV^-}$	$(\mu\text{s})^{-1}$	NV^- fluorescence rate
$K_{NV^0}^{(f)}$	$1/\tau_{NV^0}$	$(\mu\text{s})^{-1}$	NV^0 fluorescence rate
K_{35}	7.9	$(\mu\text{s})^{-1}$	NV^- ES $m_s=0 \rightarrow$ singlet
K_{45}	45	$(\mu\text{s})^{-1}$	NV^- ES $m_s=\pm 1 \rightarrow$ singlet
K_{56}	1000	$(\mu\text{s})^{-1}$	Singlet ES \rightarrow GS
K_{61}	6.5	$(\mu\text{s})^{-1}$	Singlet GS $\rightarrow NV^-$ GS $m_s=0$
K_{62}	0.1	$(\mu\text{s})^{-1}$	Singlet GS $\rightarrow NV^-$ GS $m_s=\pm 1$
K_{iG}	852	$(\mu\text{s})^{-1}/\text{mW}$	Ionization rate (green laser)
K_{rG}	134	$(\mu\text{s})^{-1}/\text{mW}$	Recombination rate (green laser)
K_{iIR}	1.2	$(\mu\text{s})^{-1}/\text{mW}$	Ionization rate (IR laser)
K_{rIR}	3.17	$(\mu\text{s})^{-1}/\text{mW}$	Recombination rate (IR laser)
laser_green_power	0.7	mW	Green laser power

- [19] L. W. Russell, S. G. Ralph, K. Wittick, J. P. Tetienne, D. A. Simpson, and P. J. Reece, Manipulating the quantum coherence of optically trapped nanodiamonds, *ACS Photonics* **5**, 4491 (2018).
- [20] N. Aslam, G. Waldherr, P. Neumann, F. Jelezko, and J. Wrachtrup, Photo-induced ionization dynamics of the nitrogen vacancy defect in diamond investigated by single-shot charge state detection, *New Journal of Physics* **15**, 10.1088/1367-2630/15/1/013064 (2013).
- [21] P. Ji and M. V. G. Dutt, Charge state dynamics of the nitrogen vacancy center in diamond under 1064-nm laser excitation, *Phys. Rev. B* **94**, 024101 (2016).
- [22] N. D. Lai, O. Faklaris, D. Zheng, V. Jacques, H.-C. Chang, J.-F. Roch, and F. Treussart, Quenching nitrogen-vacancy center photoluminescence with an infrared pulsed laser, *New Journal of Physics* **15**, 033030 (2013).
- [23] I. Meirzada, Y. Hovav, S. A. Wolf, and N. Bar-Gill, Negative charge enhancement of near-surface nitrogen vacancy centers by multicolor excitation, *Physical Review B* **98**, 245411 (2018), arXiv:1709.04776.
- [24] K.-M. C. Fu, C. Santori, P. E. Barclay, L. J. Rogers, N. B. Manson, and R. G. Beausoleil, Conversion of neutral nitrogen-vacancy centers to negatively charged nitrogen-vacancy centers through selective oxidation, *Applied Physics Letters* **96**, 121907 (2010).
- [25] M. Janik, M. Głowacki, M. Sawczak, A. Wcisło, P. Niedziakowski, K. Jurak, M. Ficek, and R. Bogdanowicz, Poly-l-lysine-functionalized fluorescent diamond particles: ph triggered fluorescence enhancement via surface charge modulation, *MRS Bulletin* **47**, 1011 (2022).
- [26] A. A. Al-Azzam N, Micropatterning of cells via adjusting surface wettability using plasma treatment and graphene oxide deposition., *PLoS ONE* **17**, 6 (2022).
- [27] M. Niora, F. Kalantarifard, A. Dervillez, A. Dezerces, A. Huck, A. Mzyk, and K. Berg-Sørensen, Biosensing with NV-centers in optically trapped nanodiamonds, in *Optical Trapping and Optical Micromanipulation XXI, Proceedings of SPIE Vol 13122* (2024).
- [28] K. C. Neuman and S. M. Block, Optical trapping, *Review of Scientific Instruments* **75**, 2787 (2004).
- [29] P. H. Jones, O. Marago, and G. Volpe, *Optical Tweezers. Principles and Applications* (Cambridge University Press, 2015).
- [30] A. Gennerich, *Optical Tweezers. Methods and Protocols, in Methods in Molecular Biology*, Vol. 1486 (Springer, 2017).
- [31] A. Ashkin, J. M. Dziedzic, J. Bjorkholm, and S. Chu, Observation of a single-beam gradient force optical trap for dielectric particles, *Optics Letters* **11**, 288 (1986).
- [32] P. Qian, Y. Zhai, J. Hu, R. Zheng, B. Chen, and N. Xu, Multicolor-illuminated charge-state dynamics of the nitrogen-vacancy center in diamond, *Phys. Rev. A* **106**, 033506 (2022).
- [33] V. M. Acosta, E. Bauch, M. P. Ledbetter, A. Waxman, L.-S. Bouchard, and D. Budker, Temperature dependence of the nitrogen-vacancy magnetic resonance in diamond, *Science Advances* **10.1103/PhysRevLett.104.070801** (2009).
- [34] D. M. Toyli, D. J. Christle, A. Alkauskas, B. B. Buckley, C. G. Van de Walle, and D. D. Awschalom, Measurement and control of single nitrogen-vacancy center spins above 600 k, *Physical Review X* **2**, 031001 (2012).
- [35] R. Chapman and T. Plakhotnik, Photoluminescence microscopy of nanodiamonds using a parabolic mirror, *Optics Letters* **36**, 1162 (2011).
- [36] H. Goudarzi, A. A. Rahman, and H. Zarrabi, Comprehensive analysis of charge state dynamics and spin decoherence in nv centers in diamond, *Physical Review B* **100**, 064105 (2019).
- [37] S. Karaveli, O. Gaathon, A. Wolcott, R. Sakakibara, O. Shemesh, D. S. Peterka, N. Osheroff, R. Yuste, and S. O'Brien, Modulation of nitrogen vacancy charge state and fluorescence in nanodiamonds using electrochemical potential, *Proceedings of the National Academy of Sciences* **113**, 3938 (2016).
- [38] F. P. Martinez, A. C. Nusantara, M. Chipaux, S. K. Padamati, and R. Schirhagl, Nanodiamond relaxometry-based detection of free-radical species when produced in chemical reactions in biologically relevant conditions, *ACS Sensors* **5**, 3090 (2020).

- [39] L. Rondin, G. Dantelle, A. Slablab, *et al.*, Surface-induced charge state conversion of nitrogen-vacancy defects in nanodiamonds, *Physical Review B* **82**, 115449 (2010).
- [40] V. M. Acosta, E. Bauch, M. P. Ledbetter, *et al.*, Temperature dependence of the nitrogen-vacancy magnetic resonance in diamond, *Physical Review Letters* **104**, 070801 (2010).